IOP Publishing Smart Materials and Structures
Smart Mater. Struct. **25** (2016) 025003 (10pp) doi:10.1088/0964-1726/25/2/025003

Stimuli dependent impedance of conductive magnetorheological elastomers

Yu Wang, Shouhu Xuan, Bo Dong, Feng Xu and Xinglong Gong

CAS Key Laboratory of Mechanical Behavior and Design of Materials, Department of Modern Mechanics, University of Science and Technology of China, Hefei 230027, People's Republic of China

E-mail: gongxl@ustc.edu.cn and xuansh@ustc.edu.cn

Received 22 May 2015, revised 18 November 2015
Accepted for publication 30 November 2015
Published 22 December 2015

Abstract

The structure dependent impedance of conductive magnetorheological elastomers (MREs) under different loads and magnetic fields has been studied in this work. By increasing the weight fraction of iron particles, the conductivity of the MREs increased. Dynamic mechanical measurements and synchrotron radiation x-ray computed tomography (SR-CT) were used and they provided reasons for the electrical properties changing significantly under pressure and magnetic field stimulation. The high sensitivity of MREs to external stimuli renders them suitable for application in force or magnetic field sensors. The equivalent circuit model was proposed to analyze the impedance response of MREs and it fits the experimental results very well. Each circuit component reflected the change of the inner interface under different conditions, thus relative changes in the microstructure could be distinguished. This method could be used not only to detect the structural changes in the MRE but also to provide a great deal of valuable information for the further understanding of the MR mechanism.

Keywords: magnetorheological elastomer (MRE), impedance spectra, equivalent circuit, microstructure

(Some figures may appear in colour only in the online journal)

1. Introduction

Magnetorheological elastomers (MREs) are mainly composed of ferromagnetic particles dispersed within polymer composites, in which the ferromagnetic particles usually distribute as a chain-like structure since the magnetic field has been applied during the prestructure process. The microstructure of an MRE, especially the direction, diameter, length of the chain and the interface between the particles and the matrix, plays a critical role in determining its mechanical behaviors [1–3]. If a mechanical loading or magnetic field loading was applied on the MRE, the particles would change their location and the chains would be deformed [4–6], thus further affecting the rheological properties.

Composite materials constructed by dispersing conductive fillers within a polymer matrix often exhibited typical conductive characteristics. Various conductive fillers, such as graphite particles [7, 8], metal particles [9–13], metal coated fillers [14, 15], carbon nanotube [16, 17] and so on, were selected to improve the electrical conductive properties of composite materials. All of them presented an obvious threshold for the formation of the three-dimensional conductive network structure in the matrix and the electroconductivity originated from the Payne effect [14, 18]. Conductive iron particles are the most commonly used ferromagnetic particles in MREs. Because they often assemble in a column-like structure, most MREs are electroconductive. It was reported that the magnetic resistance of an MRE is sensitive to the structural change induced by the externally applied strain because of the typical piezoelectric characteristics in the conductive polymer composite. Moreover, the microstucture of the MRE is also influenced by the external applied magnetic field, thus the relative structural dependent conductivity is also sensitive to the magnetic field. To this end, the investigation into conductive MREs has attracted increasing interest due to their potential applications in sensors.

The sensitivity of the MRE was influenced by volume fraction and the MR suspension proportion [19]. With the addition of carbon blacks into the matrix, the mechanical

properties and conductive properties were improved significantly [20]. When voltage was loaded, the output terminals of the magnetorheological sensor device are considerably influenced by the intensity of the transverse magnetic field and by the intensity I_c of the control current, respectively [21–26]. The electrical resistance of the MRE-hybrid in a certain transverse magnetic field of intensity was measured under a certain compression pressure, and the dependence between resistance, magnetic field intensity and compression pressure was determined. A new dimensionless number [27], N, was defined as the ratio of the magnetic force to the elastic force inside an MRE. It was found that the electrical resistivity of MREs was only dependent on the total strain due to the applied magnetic flux density and/or applied mechanical compression loads. Moreover, to improve the sensing capability, the graphite doped MRE was developed [28]. With increased graphite weight fraction or magnetic field, the sensitivity increased. To take advantage of these properties, the MREs were embedded in the sandwich beam to adjust the stiffness and fundamental frequency of the system, and mathematical modeling was carried out to obtain the equation of motion and determine the system parameters [29, 30]. The dynamic stability of a symmetric sandwich beam with an MRE embedded viscoelastic core and conductive skin subjected to axial periodic loads has been investigated using the finite element method [31].

In addition, it was too difficult to detect, using the traditional techniques such as TEM, SEM [1, 32, 33], x-ray [34–36] and so on, the structural changes of the MRE under the application of external strain or magnetic field. Considering the electroconductive properties were very sensitive to the chain-like aggregations composed of iron particles, the investigation of the loading or magnetic field dependent conductivity of the MREs was not only important for analyzing the MR sensing but also essential for detecting the inner states of the MRE. The impedance spectra (IS) technique is a powerful tool for studying the electroconducting properties by testing the interface behavior between electrode and electrolyte. Xu *et al* [37] reported that the IS of the MR materials were dependent on the aggregation structures. As the angle between the particle chains and the testing direction was decreased, the resistance increased, thus an equivalent electrical method was developed to quantitatively characterize the anisotropy of the magnetorheological plastomer (MRP). Wang *et al* [38] also investigated the sensing properties of MREs by using the IS technique. An excitation voltage over a range of frequencies was applied to the specimens, and the resistance in response to compressive deformation and applied magnetic field, as well as the impedance response of the MRE under different magnetic fields, were studied. However, the impedance spectroscopies of MREs under different external loading and the reasons for the relative change in the microstructure have not been studied and explained, and this is what we focus on in this paper.

In this paper, we investigate the impedance change of the MRE samples under different external loading. After building an equivalent circuit model, all parts of the circuit components were presented and analyzed. The result shows that a tiny change in the microstructure or damage on the interface layer could greatly influence the impedance spectroscopy of an MRE. On the basis of the experimental results, a new quick and nondestructive method was developed to characterize the degree of the microstructure change.

2. Experimental section

2.1. Preparation of MREs

The natural rubber (NR, type SCR WF) produced by Hainan Rubber Group in China was used as the matrix of the MREs. The magnetic particles were carbonyl irons (CI, type CN) with an average diameter of 6 μm, produced by BASF. The rosin glycerin [39] ester was provided by West Tech Chemical Co. Ltd in China. Plasticizers were composed of half dimethyl phthalate and half white vaseline. The sulphur was chosen as the vulcanizer. All the reagents were analytically pure and were used without additional purification.

Considering the simplicity and accuracy of building the model and analyzing it, there are no more conductive materials added in the MRE except carbonyl iron powder particles, 85 wt% fraction of iron particles were selected to keep a proper space between adjacent iron particles in MRE, so as to ensure a good conductivity and a clear feedback when loading pressure or external magnetic field. Typically, all the components were homogeneously mixed by using a two-roll mill (Taihu Rubber Machinery Inc. China, Model XK-160), and then compressed into a columnar model with a height of 20 mm and a diameter of 10 mm. The mixtures were prestructured under an external magnetic field of 1.5 T and an environmental temperature of 80 °C for 15 min. Finally, the MREs were obtained after being cured for 20 min at a temperature of 153 °C. The direction of the magnetic field was perpendicular to the bottom surface of the cylindrical MREs. Therefore, the CI particles assembled to form chain-like structures in the matrix.

2.2. Test system and methods

The dynamic mechanical properties of samples were measured by using a modified dynamic mechanical analyzer (DMA). In this system, a self-made electromagnet which can generate a variable magnetic field was attached to a normal DMA (Triton Technology Ltd, UK, model Tritec 2000B). In this research, the MRE samples had dimensions of 10 mm × 10 mm × 5 mm, and the particle chains were parallel to the thickness direction. The testing magnetic field was swept from 0 mT to 800 mT, and the testing frequency was swept from 1 Hz to 16 Hz. In addition, the shear strain amplitude was set at 0.1%.

The SR-CT experiment was performed on the BL13W1 beamline in the Shanghai synchrotron radiation facility. The samples were placed at a distance of 14 cm from the CCD camera (14 bit dynamic, 2048 × 2048 pixel array), which yielded a pixel size of 0.16 μm. 720 radiographs were taken at regular increments over 180° of rotation, each with an exposure time of 1 s and a beam energy of 15 keV.

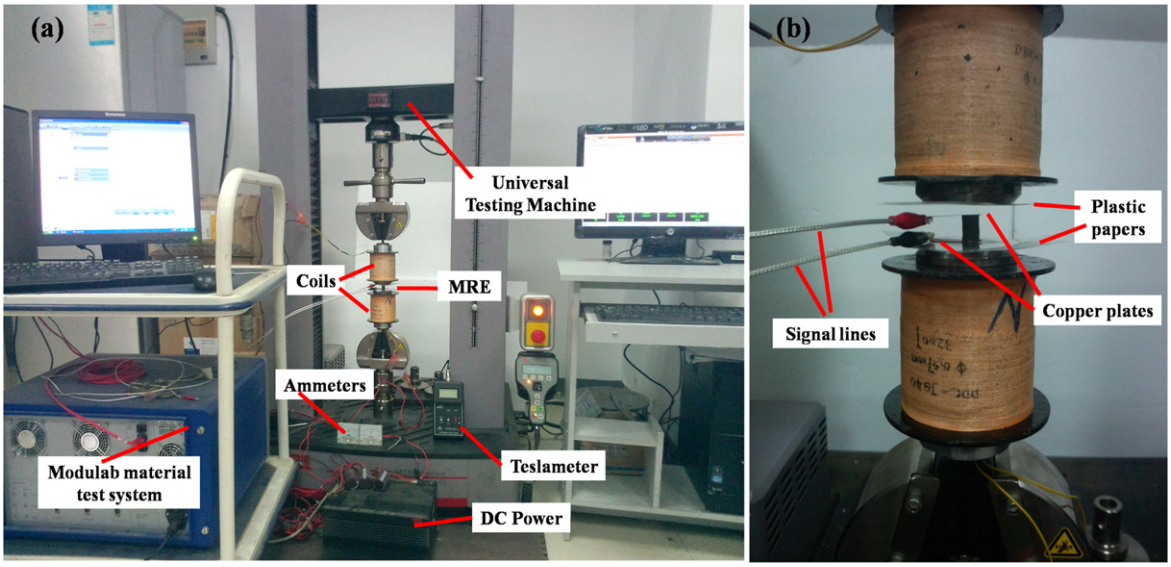

Figure 1. The electrical test system (a) and the placement details of the MRE sample (b).

In addition, an electrical test system and an effective test method were set up. Because of the low electrical conductivity in the bottom surfaces of the cylindrical MREs, it was conglutinated with two copper polar plates after cutting about 1 mm off the bottom surfaces. It was sensitive enough that MREs could maintain a stable conductivity if micro gaps existed, even they could not be observed by the naked eye, so the conductive adhesives (Shanghai Research Institute of synthetic resins, China, Type DAD-40) were used to connect MREs and copper plates, and the connection process was conducted for 24 h under a certain pressure at room temperature. In this case, the micro gaps between the sample and polar plates were filled with conductive adhesives. By the way, the oxide layers on the surface of copper plates should be polished using abrasive paper. Although they were very thin, they exhibited a great impact on the measurement of the impedance spectroscopy.

Figure 1 shows the electrical test system, in which two signal lines with shielding layers were used to connect copper polar plates and the Modulab material test system (MTS, Solartron analytical, AMETEK advanced measurement technology, Inc, United Kingdom). This system can generate an excitation voltage and measure the response voltage or current. As it is connected to the computer, various types of testing can be controlled by the computer. Two magnetic field generators composed of a coil and an iron core were designed, and the magnetic field can be obtained by adjusting the current. The magnetic field generators were fixed using the clamps of the Electromechanical Universal Testing Machine (Model 43, MTS System Corporation, China), and the MRE sample was set between the iron cores. The stress loaded on the MRE was controlled by the computer and the relationship between force and displacement was measured. The gap between the coils and the intensity of current were adjusted constantly, so a teslameter (type HT20, Shanghai Hengtong magnetic technology Co., Ltd, China) was used to measure the magnetic flux density. Several plastic papers were pasted onto the surfaces of the iron cores to insulate the MRE sample.

In this research, the core module of the Modulab material test system was used. The electrical response was independent of the amplitude of the excitation voltage under a certain range. So an alternating current (AC) voltage amplitude was set at 2000 mV and this avoided some of the data jitter caused by the power source. There was no DC voltage excitation superimposed. If the AC voltage amplitude was set to be smaller, some data jitter would be measured when the frequency swept to approximately 50 Hz . This was due to the frequency of the excitation voltage; the AC voltage from the power source in China reached the same value and the resonance occurred [37].

The frequency of the AC was set to sweep from 1000 kHz to 1 Hz, and the Universal Testing Machine was set to load stress on the MREs from 0 N to 45 N. During each measurement, the stress was firstly loaded onto the MREs for 2 min until it became stable, and then the testing was conducted. Then the impedance spectroscopy test was conducted. When stress loading reached a critical value, the microstructure of the MREs significantly changed. In particular, the interface between the CI particles and the NR rubber would be changed and even destroyed. Therefore, all the samples were repeatly measured to collect data.

3. Result and discussion

The relationship between shear storage modulus and magnetic field strength is shown in figure 2. Because of the high content of iron particles, the shear modulus increases greatly as the magnetic field strength is raised. At a shear frequency of 1 Hz, for instance, the storage modulus increases from 5.14 MPa to 19.05 MPa, and the MR effect reaches 270.8%. In addition, the increase in shear frequency leads to the corresponding improvement of the storage modulus. As

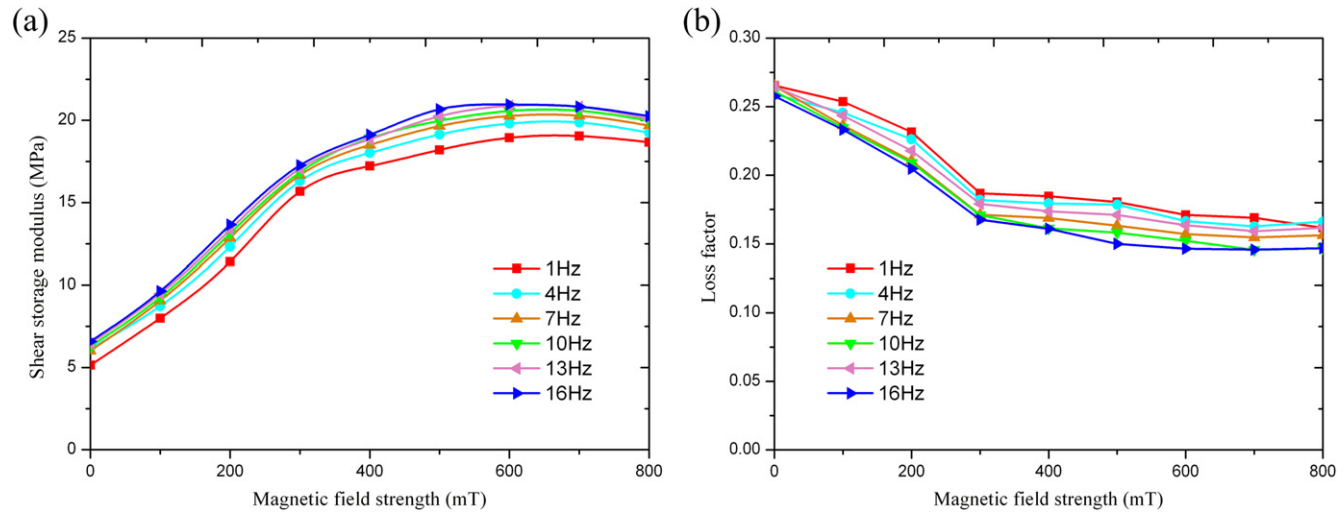

Figure 2. Magnetic field strength dependency of shear storage modulous (a) and loss factor (b) of MRE samples under different frequencies.

figure 2(b) shows, the loss factor displays decreasing tendencies. At a shear frequency of 1 Hz, the loss factor decreases from 0.27 to 0.16. As the magnetic field strength increases, the loss factors display different tendencies: a fast decreasing tendency when the magnetic field strength is less than 300 mT, and then a slowly decreasing tendency. Both the high shear modulus and the marked change in the loss factor at a low magnetic field strength reflects that the interparticle spacing of the iron particles is small enough. In this case, a further change in the microstructure would have obvious feedback on the electrical performance measurements.

Dynamic mechanical properties of MRE samples are usually measured using a dynamic mechanical analyzer (DMA) or rheometer, but the deformation caused by stress loading during the test will change the microstructure and destroy the interface layer. In addition, the mechanical loadings are long and frequently applied to the MREs, so it is impossible to use conventional measuring methods to judge the change in the microstructure and mechanical properties. For microstructure characterization, the impedance spectroscopy is proven to be an appropriate detecting method. Without destroying the microstructure and surface layers, the electrical properties can be measured in real time, which is favored for detecting the micro deformations or destructions of the MREs' structures.

Figure 3 shows the Nyquist plots of MREs under different press loading without applying the magnetic field. The Nyquist plot expresses the relationship between the real part and the imaginary part of the impedance spectroscopy, especially with regard to discussing the electrode-materials' interface properties and conductive mechanism. Figure 3(a) shows the Nyquist plot of MREs under zero magnetic field and stress loading. The curve presents a short period of arc at high frequency, and then shows a bigger semicircle when the frequency sweeps to medium and low frequency. Here, the short period of arc at high frequency relates to the fabrication of MREs. The inevitable difference in the MREs' microstructure caused by the fabrication is presented by the impedance spectroscopy measurement, and the curves of different samples are not always the same at high frequency. Because of the slight variance in space distribution between the adjacent iron particles, and the subtly different bonding degrees of the interface between iron particles and the natural rubber, microcapacitors form and result in the different electrical response at high frequency excitation AC. These parts of the capacitors are broken down or come through under AC and the influence of the impedance decreases at high frequency, so the curves have a short period of arc when the real part values of the impedance spectroscopy are lower.

By increasing the pressure from 0 N to 45 N, the short period of arc at high frequency gradually disappears and is integrated into the bigger capacitive impedance loop by degrees, which is caused by the charge transfer. In other words, both the effects of interfacial capacitors between the MRE and the polar plates and the effects of the capacitors formed between the adjacent iron particles are reduced, or even disappear, with increasing pressure load under the excitation of high frequency AC. Under a certain compression, the distance between iron particles is reduced. The difference between these distances and the original partial microstructures becomes more and more inconspicuous. Anisotropic MREs tend to be isotropous, and the unity of the whole MRE result in the short period of arc integrated into the bigger capacitive impedance loop, until the Nyquist plot becomes a semicircle. When the stress is larger, the semicircle of the capacitive impedance loop can be completed if the test frequency of the excitation AC is high enough. The missing part of the semicircle is due to the wave crest of the phase angle moved towards the direction of high frequency until its corresponding frequency exceeds 10^6 Hz (the upper limit of the test system).

The real part of the Nyquist plot contracted when the excitation AC was at low frequency. The degree of the contraction increased with the pressure. We extracted the

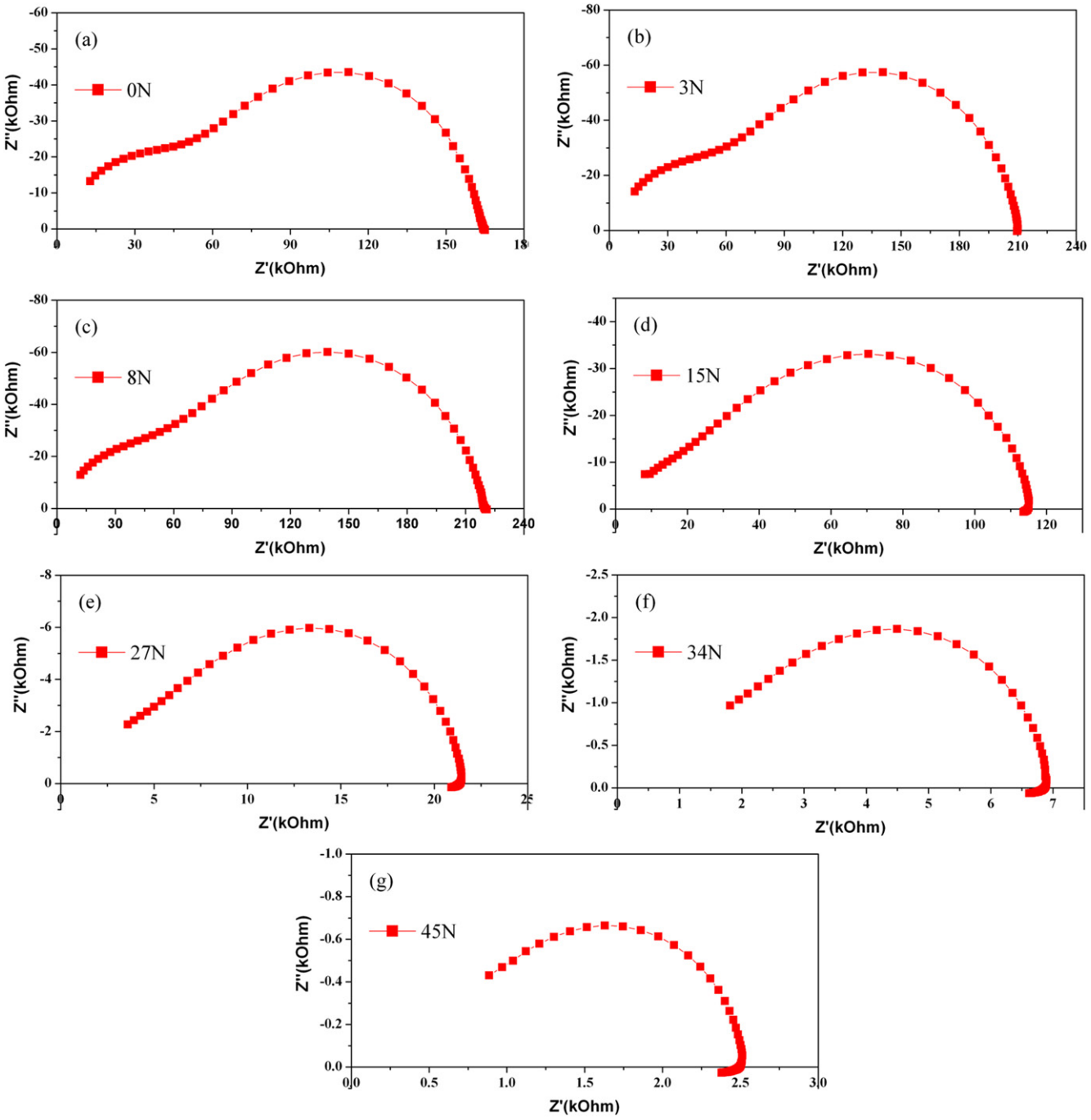

Figure 3. Nyquist plots of MREs under different press loading without magnetic field: 0 N (a), 3 N (b), 8 N (c), 15 N (d), 27 N (e), 34 N (f), 45 N (g).

contraction, and defined the coefficient R_d as

$$R_d = \frac{|Z'_c|}{Z'_{max} - Z'_{min}}, \quad (1)$$

where $|Z'_c|$ means the contracted part corresponding to the length of the real part, and $Z'_{max/min}$ means the maximum/minimum resistance that appeared during the frequency sweeping. Through the coefficient of R_d, the change, or even the degree of damage, of the microscopic structure of the MREs could be defined. The bigger the coefficient R_d, the more microstructure damage. As shown in figure 4, with increasing pressure, R_d increased from 0.002 to 0.095 when magnetic field was 300 mT. If the magnetic field was weak, such as 0 mT, R_d started to rise after the pressure load reached 8 N. Increasing the magnetic field further, this part of the pressure decreased until it disappeared. After improving the magnetic field, the growth rate of R_d was higher at the beginning of the load, and in all cases the growth rate of R_d showed the tendency to first rise and then reduce. In analyzing the impedance spectrum, the data were generally deleted if the imaginary part was positive. However, this region of curves could be considered separately in measuring the electric properties of MREs, as a test method to judge the

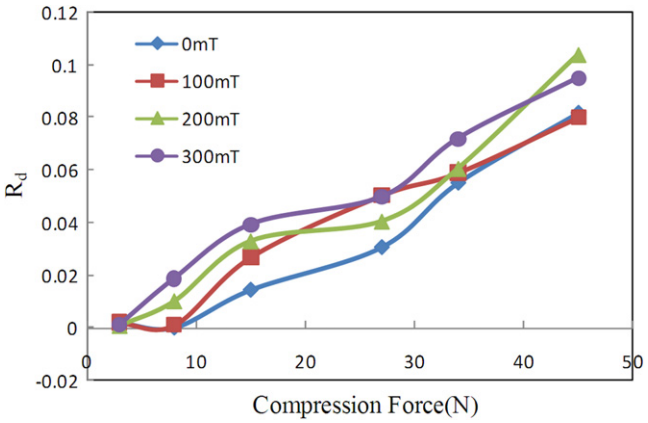

Figure 4. The contraction coefficient R_d of the real part of the Nyquist plot under different compression forces.

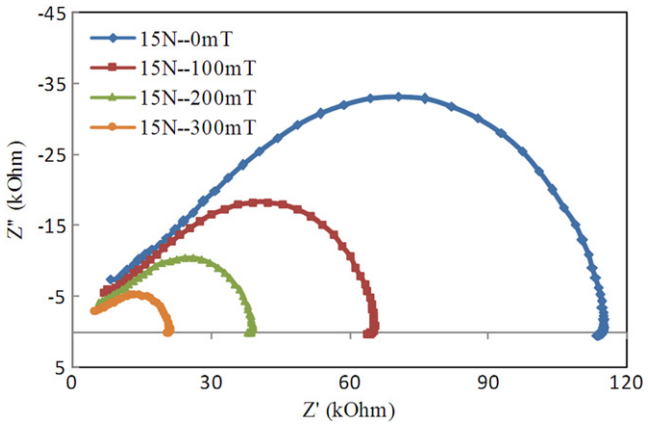

Figure 5. Nyquist plots of MREs under different magnetic fields when the pressure load was 15 N.

combination of the interface between particles and matrix. If MRE samples were placed for a long time, or were loaded with tensile or compressive deformations, the contraction of the real part would be more obvious.

Besides the pressure, the magnetic field also exhibited a high influence on the electrical properties of the MREs. Figure 5 shows the relative impedances under the application of the magnetic field from 0 mT to 300 mT when the pressure load is 15 N. Increasing the magnetic field intensity, the maximum real part of the impedance spectroscopy decreases from 115 kOhm to 21 kOhm, in other words, conductivity increases greatly. Meanwhile, the imaginary part decreases accordingly. In addition, the contraction of the real part appears. The mechanical loading has a great influence at the high frequency area of the Nyquist plot, however, when the magnetic field is loaded, this change is not obvious. The shapes of the curves are similar and they reflect the magneto shrinkage properties of MREs. The external compression deformation caused by the pressure easily leads to the relative slippage and destruction of the interface layer between the particles and matrix. However, they are not easily destroyed by the magneto shrinkage properties caused by the movement of the magnetic particles under magnetic field stimulation. Therefore, the change of the region at high frequency was not obvious when the magnetic field was applied. This phenomenon also confirmed that the method of using AC to measure the impedance spectroscopy was sensitive to the MREs' microstructure.

An equivalent circuit model was built to analyze the impedance response of MREs under mechanical loading and magnetic field stimulation (figure 6). The equivalent circuit consists of a resistance R_1 in parallel with a constant phase element CPE_1, and another resistance R_2 in parallel with CPE_2. The impedance of CPE was defined as:

$$Z_{CPE} = A^{-1}\left(j\omega^{-P}\right), \tag{2}$$

where $j = \sqrt{-1}$ and ω represents the angular frequency. A was always written as CPE-T and P was always written as CPE-P during the analysis of the equivalent circuit model. Both A and P are fitting parameters. The actual situation of the MREs' Nyquist plots were too difficult to fit through ideal circuit elements, so the constant phase angle element, CPE, was introduced. In the equation, A represents the capacitance of the corresponding capacitors and P represents the degree of similarity to an ideal capacitor, and the range of P is from 0 to 1. $P = 0$ means the CPE is a resistance, if $P = 0.5$ the CPE becomes a Weber impedance, and if P reaches 1 the CPE is an ideal capacitor. The resistances R_1 and R_2 represent the electrode-sample interface resistance and the resistance of the MRE sample itself along the direction of the current and magnetic field, respectively. The respective corresponding physical interpretations of R_1 and R_2 could be distinguished separately after comparing the values and analyzing the curves of CPE-T. The MREs' impedance spectrums of the Nyquist plots under different pressure loads fit well with this equivalent circuit model (figure 6) and each part of the component parameters can be obtained. The advantage of using the equivalent circuit model was that the real parameters of the samples could be extracted from the data measured.

As shown in figure 7, the maximum of R_2 was larger than for R_1. When the magnetic field was 0 mT, the maximum of R_2 reached 150.4 kOhm, but R_1 only reached 72.1 kOhm. So it could be considered that R_2 represents the resistance of the MRE sample caused by the gap between magnetic particles, while the smaller R_1 represents the resistance of the electrode-sample interface layer. Zhu *et al* [40] found that the conductivity of the MREs increased with increasing pressure, and they provided the equation to calculate the relative conductivity. However, in this study, under different magnetic field conditions, R_1 and R_2 had a significant decrease when the force was larger than 8 N. Interestingly, at the beginning of the pressure load, R_1 and R_2 had an obvious rising process. When the magnetic field was 0 mT, R_2 rose from 104.1 kOhm to 150.4 kOhm. In other words, the conductivity of the MRE samples decreased, in contrast with the pressure increase when it was low.

In order to analyze the relationship between the microstructure and the change the electrical performance, synchrotron radiation x-ray computed tomography (SR-CT) was used to study the inner structure of the MRE (figure 8). Here, the framework of the cuboid is the boundary of the CCD

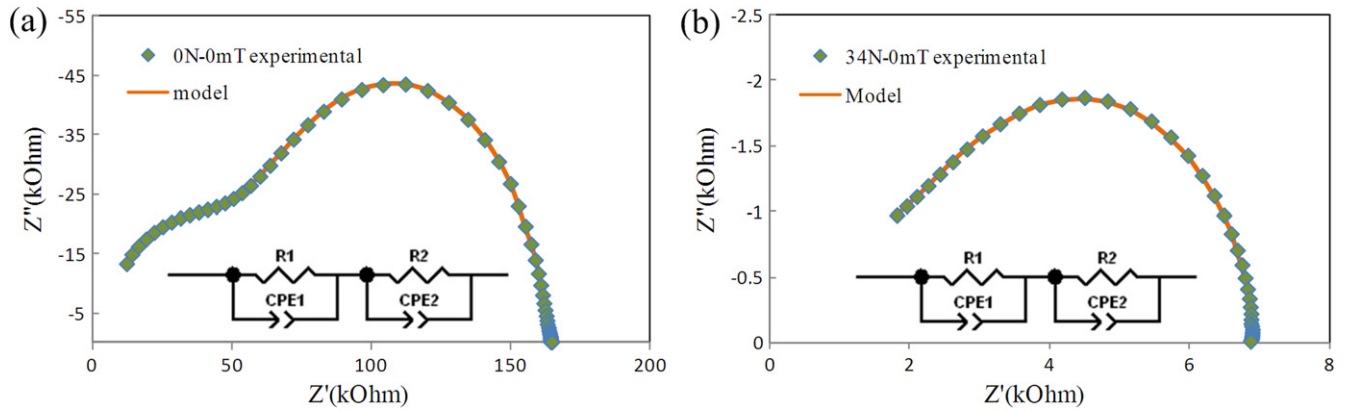

Figure 6. Two typical shapes of Nyquist plots of MREs under different pressure loads and the fitting results used in the equivalent circuit model: (a) 0 N; (b) 34 N.

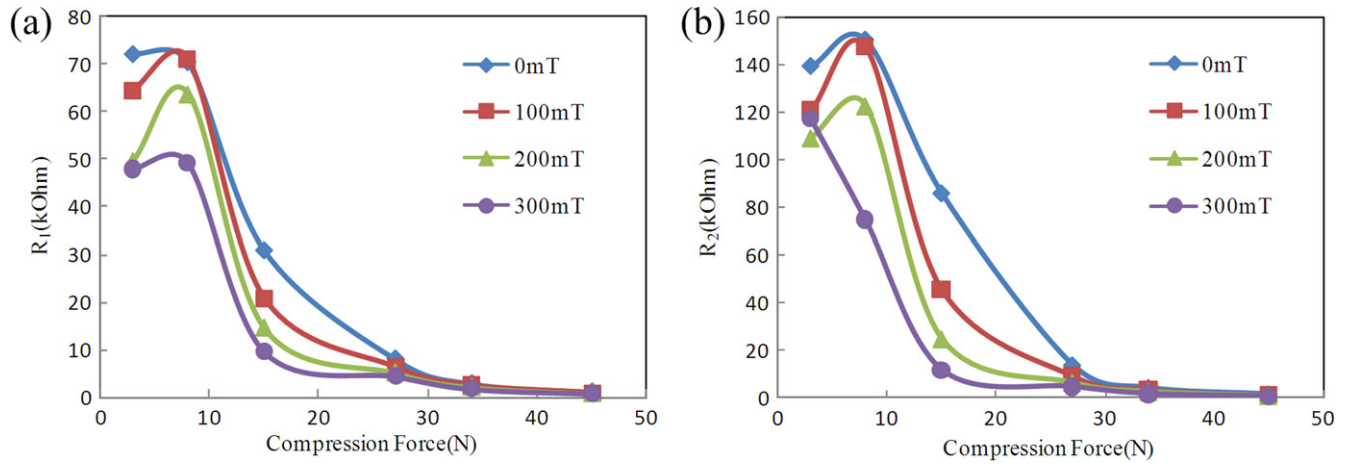

Figure 7. The resistance elements R_1 (a) and R_2 (b) under different compression forces and magnetic fields.

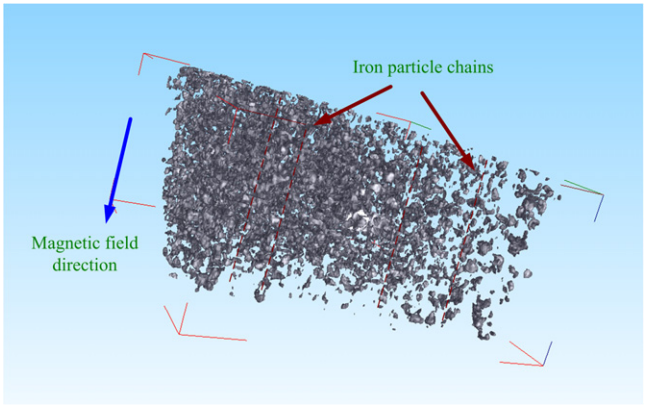

Figure 8. SR-CT 3D images of MRE with 85 wt% iron particles under 0 MPa load.

view. In comparison to the traditional TEM and SEM methods, SR-CT is an advanced and effective technique to directly observe microstructures in materials, nondestructively, in three dimensions (3D) [41, 42]. Figure 8 shows the SR-CT 3D morphology image of an MRE under a load of 0 MPa. For clarity, the image shows only the iron particles after removing the natural rubber signal by image filtering. The particle chain structures, which were parallel to the external magnetic field direction, were formed in the matrix and the final three-dimensional MRE composite was obtained. Because of the high content of iron particles, the particle chains are close to each other and seem concentrated.

With increasing pressure, the resistance changed due to the iron particles getting close and even contacting each other. Simultaneously, the microstructure deformed and relative displacement occurred at interface layers between the particles and the matrix (figure 9). Under low pressure, the latter reason was slightly dominant, so the resistance slowly rose. Because the mass fraction of iron power reached 85%, the former reason played a dominant role soon after the pressure reached a critical value, and the resistance decreased quickly and tends to stablise gradually. As shown in figure 7(b), the resistance of R_2 decreased once the pressure was loaded when the intensity of the magnetic field was at 300 mT. The reason for this was that the iron particles were close enough to each other, which was caused by magneto contraction. However, on the electrode-sample interface layer there were few particles, so the resistance still had a rising trend. In general electrical tests, the samples were often tested under a certain pressure, but there was no basis or interpretation as to how much pressure should be loaded. This research indicated that the optimum pressure during the measurement was the one

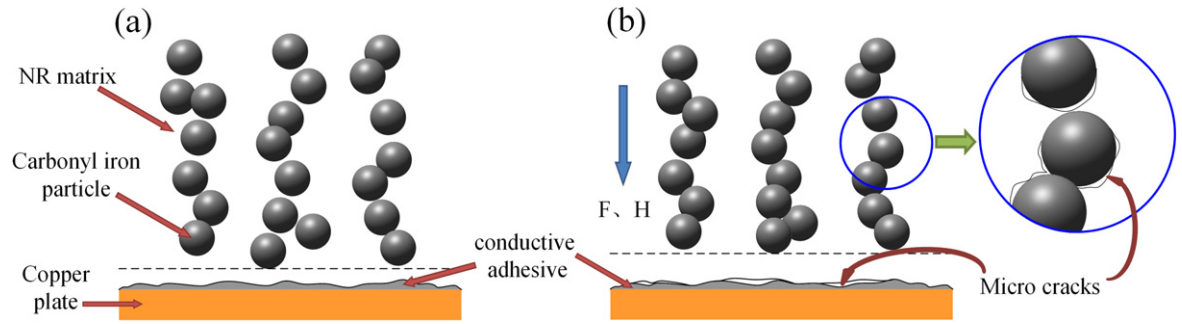

Figure 9. Schematic of MRE's microstructure change under pressure load and magnetic field.

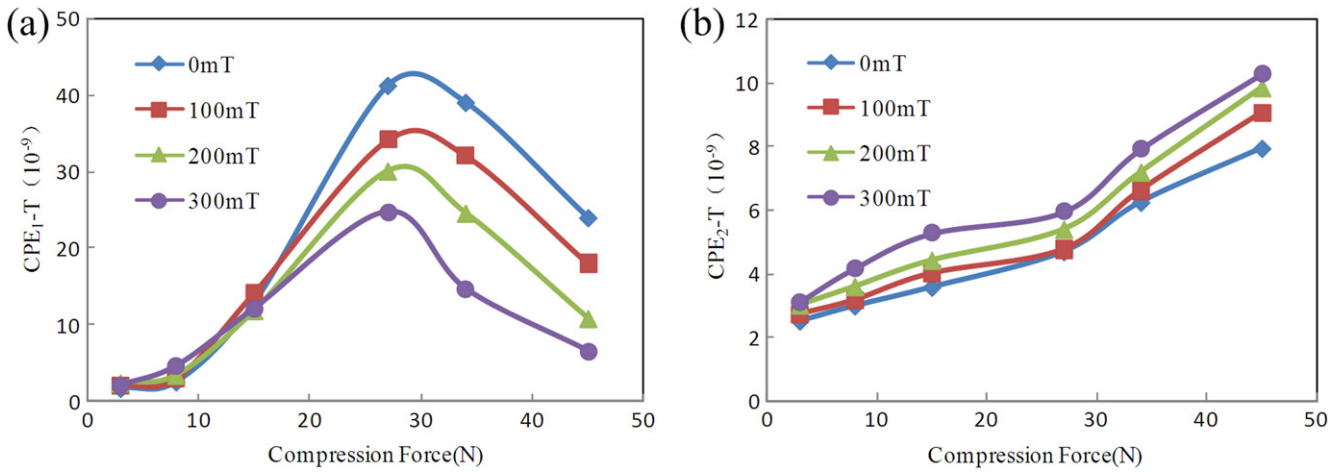

Figure 10. The constant phase angle element CPE_1-T (a) and CPE_2-T (b) under different compression forces and magnetic fields.

which lead resistance R_2 to reach the maximum value. In this case, the samples and plates fit closely enough if conductive glue is not used. Moreover, the microstructure tends to a balance under the influence of the two factors.

The physical mean of the resistances R_1 and R_2 can also be obtained through analyzing the parameter CPE-T. The constant phase angle element was generally used to describe the surface roughness of the interface. In this work, the surface roughness of the micron-sized iron particles could be neglected, so the change of the parameters was mainly effected by the particle distribution. Increasing the pressure, CPE_1-T firstly increased before the compression force reached 27 N, and then reduced, while CPE_2-T only exhibited an increasing tendency. Similarly, with the increase of the magnetic field intensity, the CPE_1-T decreased gradually while CPE_2-T was rising. Therefore, R_1 and CPE_1 represented the interface part between the MRE samples and copper plates, while R_2 and CPE_2 represented the part of the MRE itself. Because the particles get close to each other, the capacitance caused by conductive particles adjacent in MREs increased along with the pressure or magnetic field. From figure 10(a), it was found that the capacitances formed by particles and plates with conductive adhesive were much larger than the ones of iron particles in MRE samples. When the magnetic field was 0 mT, CPE_1-T reached 41.2×10^{-9}, but CPE_2-T only reached 7.92×10^{-9}. Before pressure loading reached 27 N, the gap between the particles and the plates decreased so the capacitance rose quickly. However, after the pressure reached a certain degree, the bonding interface was broken. The microcracks directly reduced the dielectric constant of the medium and resulted in the decrease of its capacitance. The content of iron particles in the interface layer was much smaller than that in the MRE samples. As soon as the magneto contraction occurred, the particles moved far away from the plates and conductive adhesive, in contrast (figure 9), resulting in the decrease in capacitance. As a practical application, we can use this method to identify the type of interface layer fatigue or damage.

The compression force, which corresponds to the turning points of the CPE-P curves in figures 11(a) and (b), reveals the comprehensive results under the influence of R and CPR-T. As we know, the higher the CPE-P, the smoother the conductive surface. Corresponding to the MREs, the particle chain was neater if the value of CPE-P was higher. The horizontal position of the turning point in figure 11(a) shows that the resistance is mainly dependent on the change in the MREs' microstructure with external excitation. With decreasing distance between the particles and the relative displacement on the particle-matrix interface, the resistance decreases. In addition, the change in the sample-plates' microstructure with external excitation corresponds to the curves of CPE-T, which is mainly caused by the damage of the interface and the intervention of the air (figure 11(a)).

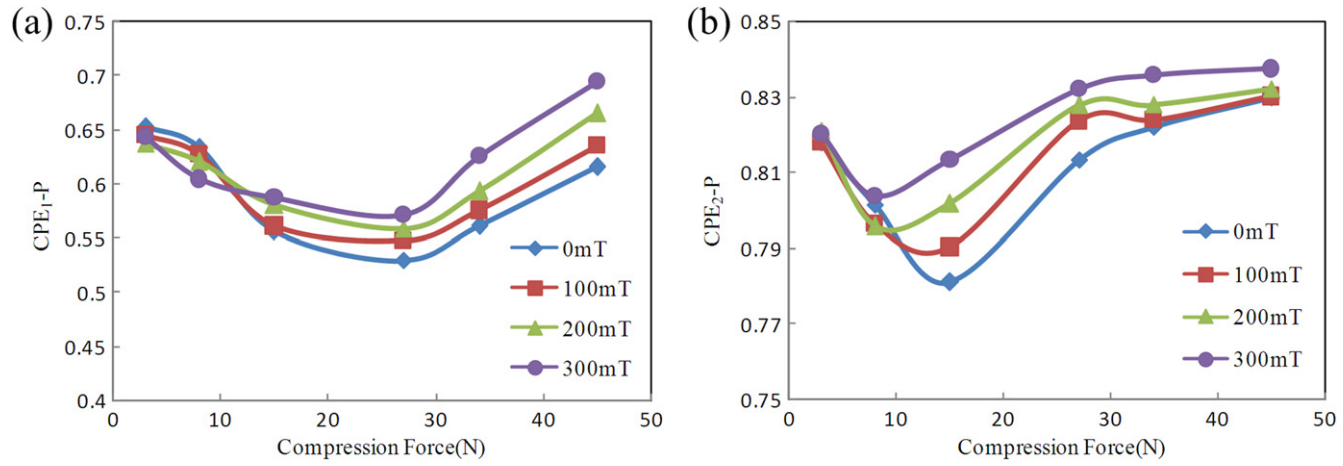

Figure 11. The constant phase angle element CPE_1-T (a) and CPE_2-T (b) under different compression forces and magnetic fields.

4. Conclusion

In this work, the impedance spectroscopy of MRE samples with 85 wt% fraction of iron particles was investigated under different magnetic fields or pressure loadings. Dynamic mechanical measurements and SR-CT were applied to study the structure dependent impedance. The results revealed that the short period of arc at high frequency in Nyquist plots is related to the fabrication of MREs, and that their differences are unavoidable. The real part of the Nyquist plot contracted when the excitation AC was at low frequency and external loading reached a certain degree. The coefficient R_d was defined to characterize the damage of the microstructure. With the pressure load increased to above 8 N when the magnetic field was low, R_d also increased, from 0 to 0.082 after calculation. The deformation caused by the magnetic field or the pressure load differed in the formation of micro-cracks. An equivalent circuit model was built to analyze the impedance response of MREs. Under 8 N the conductivity of the MRE samples decreased, in contrast to the stress increase, which provided a kind of basis regarding how much pressure should be loaded during the electrical properties tests. The constant phase angle element CPE-T was used to distinguish the physical meanings of circuit components, and CPE-P was the comprehensive results under the influence of R and CPR-T. This research can be used in the field of MRE non-destructive testing and to judge microstructure damage in real time.

Acknowledgments

Financial support from the National Natural Science Foundation of China (grant nos. 11572309, 11125210, 11572310), Anhui Provincial Natural Science Foundation of China (1408085QA17) and the National Basic Research Program of China (973 Program, grant no. 2012CB937500) are gratefully acknowledged. This work was supported by the Collaborative Innovation Center of Suzhou Nano Science and Technology.

References

[1] Fan Y C, Gong X L, Xuan S H, Qin L J and Li X F 2013 Effect of cross-link density of the matrix on the damping properties of magnetorheological elastomers *Ind. Eng. Chem. Res.* **52** 771–8

[2] Zubarev A Y and Borin D Y 2015 Effect of particle concentration on ferrogel magnetodeformation *J. Magn. Magn. Mater.* **377** 373–7

[3] Shuib R K, Pickering K L and Mace B R 2015 Dynamic properties of magnetorheological elastomers based on iron sand and natural rubber *J. Appl. Polym. Sci.* **132** 41506

[4] Han Y, Mohla A, Huang X, Hong W and Faidley L E 2015 Magnetostriction and field stiffening of magneto-active elastomers *Int. J. Appl. Mechanics* **7** 1550001

[5] Biller A M, Stolbov O V and Raikher Y L 2014 Modeling of particle interactions in magnetorheological elastomers *J. Appl. Phys.* **116** 114904

[6] Chen W W, Sun L Y, Li X H and Wang D F 2013 Numerical investigation on the magnetostrictive effect of magneto-sensitive elastomers based on a magneto-structural coupling algorithm *Smart Mater. Struct.* **22** 105012

[7] Sau K P, Chaki T K and Khastgir D 1997 Conductive rubber composites from different blends of ethylene-propylene-diene rubber and nitrile rubber *J. Mater. Sci.* **32** 5717–24

[8] Das N C, Chaki T K and Khastgir D 2002 Effect of processing parameters, applied pressure and temperature on the electrical resistivity of rubber-based conductive composites *Carbon* **40** 807–16

[9] Lee H H, Chou K S and Shih Z W 2005 Effect of nano-sized silver particles on the resistivity of polymeric conductive adhesives *Int. J. Adhes. Adhes.* **25** 437–41

[10] Jang J and Ryu S K 2006 Physical property and electrical conductivity of electroless ag-plated carbon fiber-reinforced paper *J. Mater. Process. Technol.* **180** 66–73

[11] Leng J S, Lan X, Liu Y J, Du S Y, Huang W M, Liu N, Phee S J and Yuan Q 2008 Electrical conductivity of thermoresponsive shape-memory polymer with embedded micron sized ni powder chains *Appl. Phys. Lett.* **92** 014104

[12] Kono A, Shimizu K, Nakano H, Goto Y, Kobayashi Y, Ougizawa T and Horibe H 2012 Positive-temperature-coefficient effect of electrical resistivity below melting point of poly(vinylidene fluoride) (pvdf) in ni particle-dispersed pvdf composites *Polymer* **53** 1760–4

[13] Christopoulos A, Hristoforou E and Tsamasphyros G 2012 Strain sensing capabilities of iron/epoxy composites *Smart Mater. Struct.* **21** 085030

[14] Zou H, Zhang L Q, Tian M, Wu S Z and Zhao S H 2010 Study on the structure and properties of conductive silicone rubber filled with nickel-coated graphite *J. Appl. Polym. Sci.* **115** 2710–7
[15] Novak I, Krupa I and Chodak I 2004 Electroconductive adhesives based on epoxy and polyurethane resins filled with silver-coated inorganic fillers *Synth. Met.* **144** 13–9
[16] Kim Y A, Hayashi T, Endo M, Gotoh Y, Wada N and Seiyama J 2006 Fabrication of aligned carbon nanotube-filled rubber composite *Scr. Mater.* **54** 31–5
[17] Kimura T, Ago H, Tobita M, Ohshima S, Kyotani M and Yumura M 2002 Polymer composites of carbon nanotubes aligned by a magnetic field *Adv. Mater.* **14** 1380–3
[18] Sorokin V V, Ecker E, Stepanov G V, Shamonin M, Monkman G J, Kramarenko E Y and Khokhlov A R 2014 Experimental study of the magnetic field enhanced payne effect in magnetorheological elastomers *Soft Matter* **10** 8765–76
[19] Leng J S, Huang W M, Lan X, Liu Y J and Du S Y 2008 Significantly reducing electrical resistivity by forming conductive ni chains in a polyurethane shape-memory polymer/carbon-black composite *Appl. Phys. Lett.* **92** 204101
[20] Nayak B, Dwivedy S K and Murthy K S R K 2015 Fabrication and characterization of magnetorheological elastomer with carbon black *J. Intell. Mater. Syst. Struct.* **26** 830–9
[21] Bica I, Anitas E M, Bunoiu M, Vatzulik B and Juganaru I 2014 Hybrid magnetorheological elastomer: Influence of magnetic field and compression pressure on its electrical conductivity *J. Ind. Eng. Chem.* **20** 3994–9
[22] Bica I, Liu Y D and Choi H J 2012 Magnetic field intensity effect on plane electric capacitor characteristics and viscoelasticity of magnetorheological elastomer *Colloid Polym. Sci.* **290** 1115–22
[23] Bica I 2012 The influence of hydrostatic pressure and transverse magnetic field on the electric conductivity of the magnetorheological elastomers *J. Ind. Eng. Chem.* **18** 483–6
[24] Bica I 2012 The influence of the magnetic field on the elastic properties of anisotropic magnetorheological elastomers *J. Ind. Eng. Chem.* **18** 1666–9
[25] Bica I 2011 Magnetoresistor sensor with magnetorheological elastomers *J. Ind. Eng. Chem.* **17** 83–9
[26] Bica I 2010 Magnetorheological elastomer-based quadrupolar element of electric circuits *Mater. Sci. Eng.* B **166** 94–8
[27] Ghafoorianfar N, Wang X J and Gordaninejad F 2014 Combined magnetic and mechanical sensing of magnetorheological elastomers *Smart Mater. Struct.* **23** 055010
[28] Tian T F, Li W H and Deng Y M 2011 Sensing capabilities of graphite based MR elastomers *Smart Mater. Struct.* **20** 025022
[29] Nayak B, Dwivedy S K and Murthy K S R K 2014 Dynamic stability of a rotating sandwich beam with magnetorheological elastomer core *Eur. J. Mech. a-Solid* **47** 143–55
[30] Nayak B, Dwivedy S K and Murthy K S R K 2011 Dynamic analysis of magnetorheological elastomer-based sandwich beam with conductive skins under various boundary conditions *J. Sound Vib.* **330** 1837–59
[31] Nayak B, Dwivedy S K and Murthy K S R K 2012 Multi-frequency excitation of magnetorheological elastomer-based sandwich beam with conductive skins *Int. J. Non Linear Mech.* **47** 448–60
[32] Yoon J H, Yang I H, Jeong U C, Chung K H, Lee J Y and Oh J E 2013 Investigation on variable shear modulus of magnetorheological elastomer based on natural rubber due to change of fabrication design *Polym. Eng. Sci.* **53** 992–1000
[33] Li W H and Nakano M 2013 Fabrication and characterization of pdms based magnetorheological elastomers *Smart Mater. Struct.* **22** 055035
[34] Gunther D, Borin D Y, Gunther S and Odenbach S 2012 X-ray micro-tomographic characterization of field-structured magnetorheological elastomers *Smart Mater. Struct.* **21** 015005
[35] Borbath T, Gunther S, Borin D Y, Gundermann T and Odenbach S 2012 X-μ CT analysis of magnetic field-induced phase transitions in magnetorheological elastomers *Smart Mater. Struct.* **21** 105018
[36] Gundermann T and Odenbach S 2014 Investigation of the motion of particles in magnetorheological elastomers by X-μ CT *Smart Mater. Struct.* **23** 105013
[37] Xu Y G, Gong X L, Liu T X and Xuan S H 2013 Magneto-induced microstructure characterization of magnetorheological plastomers using impedance spectroscopy *Soft Matter.* **9** 7701–9
[38] Wang X J, Gordaninejad F, Calgar M, Liu Y M, Sutrisno J and Fuchs A 2009 Sensing behavior of magnetorheological elastomers *J. Mech. Des.* **131** 091004
[39] Ge L, Gong X L, Fan Y C and Xuan S H 2013 Preparation and mechanical properties of the magnetorheological elastomer based on natural rubber/rosin glycerin hybrid matrix *Smart Mater. Struct.* **22** 115029
[40] Zhu X L, Meng Y G and Tian Y 2010 Nonlinear pressure-dependent conductivity of magnetorheological elastomers *Smart Mater. Struct.* **19** 117001
[41] Li Y C, Xu F, Hu X F, Kang D, Xiao T Q and Wu X P 2014 *In situ* investigation on the mixed-interaction mechanisms in the metal-ceramic system's microwave sintering *Acta Mater.* **66** 293–301
[42] Hu X F, Wang L B, Xu F, Xiao T Q and Zhang Z 2014 *In situ* observations of fractures in short carbon fiber/epoxy composites *Carbon* **67** 368–76